Monte Carlo simulations of stress relaxation of entanglement-free Fraenkel chains. II. Nonlinear polymer viscoelasticity

Y.-H. Lin and A. K. Das

Citation: The Journal of Chemical Physics **126**, 074903 (2007); doi: 10.1063/1.2431649
View online: http://dx.doi.org/10.1063/1.2431649
View Table of Contents: http://scitation.aip.org/content/aip/journal/jcp/126/7?ver=pdfcov
Published by the AIP Publishing

Monte Carlo simulations of stress relaxation of entanglement-free Fraenkel chains. II. Nonlinear polymer viscoelasticity

Y.-H. Lin[a] and A. K. Das
Department of Applied Chemistry, National Chiao Tung University, Hsinchu 30050, Taiwan

(Received 2 October 2006; accepted 12 December 2006; published online 15 February 2007)

The nonlinear viscoelastic behavior of the Fraenkel-chain model is studied with respect to the constitutive equation of the Rouse model. Distinctly different from the results of the Rouse model, the Fraenkel-chain model gives the following characteristic nonlinear behavior: (a) The two distinct dynamic modes in the relaxation modulus $G_S(t,\lambda)$—as observed in the linear region reported in Paper I [Y.-H. Lin and A. K. Das, J. Chem. Phys. **126**, 074902 (2007), preceding paper]—or in the first normal-stress difference function $G_{\Psi 1}(t,\lambda)$ are shown to have different strain dependences: strain hardening for the fast mode and strain softening for the slow mode. (b) The Lodge–Meissner relation $G_S(t,\lambda)=G_{\Psi 1}(t,\lambda)$ holds over the whole time range, which has been shown both analytically and by simulation. (c) The second normal-stress difference is nonzero, being positive in the fast-mode region and negative in the slow-mode region. The comparisons between orientation and stress for all tensor components consistently confirm the strong correlation of the slow mode as well as its entropic nature with the segmental-orientation anisotropy as shown in the linear region studied in Paper I. A consequence of this correlation is the applicability of the stress-optical rule in the slow-mode region. This also leads to the expectation that the damping function $h(\lambda)=G_S(t,\lambda)/G_S(t,\lambda\rightarrow 0)$ and the ratio between the first and second normal-stress differences, $N_2(t,\lambda)/N_1(t,\lambda)$, are described by the orientation tensor which has the same form as that given by Doi and Edwards [J. Chem. Soc. Faraday Trans. 2 **74**, 1789 (1978); **74**, 1802 (1978)] with independent-alignment approximation for an entangled system. The similarity between the slow mode of an entanglement-free Fraenkel-chain system and the terminal mode of an entangled polymer system as observed in the comparison of theory, simulation, and experiment suggests that the close correlation of the entropic nature of the mode with the orientation anisotropy—as of the Fraenkel segment or the primitive step in the Doi–Edwards theory—is a generally valid physical concept in polymer viscoelasticity. © *2007 American Institute of Physics*.
[DOI: 10.1063/1.2431649]

I. INTRODUCTION

In Paper I,[1] the linear viscoelastic behavior for Fraenkel chains[2] has been studied by Monte Carlo simulations, revealing two distinct dynamic modes in the relaxation modulus $G_S(t)$: The fast mode arises from the segment-tension fluctuations or reflects the relaxation of the segment tension created by segments being stretched by the applied step shear deformation—an energetic-interactions-driven dynamic process. The slow mode arises from the fluctuating segmental-orientation anisotropy or represents the randomization of the induced segmental-orientation anisotropy—an entropy-driven dynamic process. Very significantly the slow mode is well described by the Rouse theory[3–5] in all aspects: the magnitude of the modulus, the line shape, and the N (number of beads) dependence of the relaxation time. This result means that as far as the slow mode is concerned, one Rouse segment may be replaced by one Fraenkel segment, even though the latter is much stiffer than the former. Furthermore, the comparison of the simulated relaxation modulus $G_S(t)$ with experimental $G(t)$ indicates that the Fraenekel-chain model has captured the key element of energetic interactions in an entanglement-free polymer melt, allowing the relative positions in time of the glassy-relaxation process (the fast mode) and the entropy-driven Rouse relaxation (the slow mode) properly described. This overall agreement between simulation and experiment is consistent with the success of the Rouse theory in explaining the linear viscoelastic spectra of entanglement-free polymer melt systems in the low-frequency (long-time) or entropic region.[5–7] Since the natural emergence of the fast (structural-relaxation) mode on top of the slow (Rouse) mode represents a dramatic improvement in linear viscoelasticity on the Rouse model, the stress relaxations of the Fraenkel-chain model obtained from the Monte Carlo simulations in the nonlinear region may be profitably analyzed in comparison with the constitutive equation of the Rouse model.

II. CONSTITUTIVE EQUATION OF THE ROUSE MODEL

The constitutive equation of the Rouse model with each chain having N beads (corresponding to molecular weight M) is given by[4,5]

[a]Electronic mail: yhlin@mail.nctu.edu.tw

$$\boldsymbol{\sigma}(t) = ckT\int_{-\infty}^{t}\left(\frac{1}{\tau_p}\right)\sum_{p=1}^{N-1}\exp\left[-\frac{(t-t')}{\tau_p}\right]\boldsymbol{\gamma}_{[0]}(t,t')dt', \quad (1)$$

where $\boldsymbol{\gamma}_{[0]}(t,t')=\boldsymbol{\delta}-\mathbf{E}(t,t')\cdot\mathbf{E}(t,t')^{\mathrm{T}}$, with $\mathbf{E}(t,t')$ being the deformation gradient tensor between the present time t and a past time t'; c is the number of polymer chains per unit volume; and τ_p, the relaxation time of the pth mode, is given by Eq. (11) of Paper I.[1] For comparison with the Monte Carlo simulation of a single chain in the mean field, both c and kT may be set to be 1, and τ_p is expressed in terms of the time steps as given by Eq. (12) of Paper I.

Following a step shear deformation $\mathbf{E}$ at time $t=0$ [Eq. (4) of paper I], the relaxation modulus $G_S(t)$ and the first normal-stress difference function $G_{\Psi 1}(t)$ of the Rouse model, both normalized to that corresponding to a single segment, are given, respectively, as (setting $kT=1$)

$$G_S(t) = -\frac{S_{xy}}{\lambda} = -\frac{\sigma_{xy}}{\lambda c(N-1)} = \frac{1}{(N-1)}\sum_{p=1}^{N-1}\exp\left[-\frac{t}{\tau_p}\right] \quad (2)$$

and

$$G_{\Psi 1}(t) = -\frac{S_{xx}(t,\lambda)-S_{yy}(t,\lambda)}{\lambda^2} = -\frac{\sigma_{xx}(t,\lambda)-\sigma_{yy}(t,\lambda)}{\lambda^2 c(N-1)} = \frac{1}{(N-1)}\sum_{p=1}^{N-1}\exp\left[-\frac{t}{\tau_p}\right]. \quad (3)$$

The key results expected from the constitutive equation of the Rouse model may be summarized as in the following:

(1) No nonlinear effect in the shear stress relaxation; in other words, $G_S(t)$ as given by Eq. (2) is independent of strain λ.
(2) The holding of the Lodge–Meissner relation;[8] namely, as indicated by Eqs. (2) and (3), $G_S(t)=G_{\Psi 1}(t)$.
(3) The second normal-stress difference as defined by $N_2(t,\lambda)=-(S_{yy}(t,\lambda)-S_{zz}(t,\lambda))$ is zero.

These results of the Rouse model are exactly confirmed by our simulations; in Fig. 1, the strain independence of $G_S(t)$ and $G_{\Psi 1}(t)$ for a five-bead Rouse chain and the agreements of the simulation results with the theoretical Rouse curve are shown.

III. EFFECTS OF THE NONLINEAR TENSILE FORCE ON THE FRAENKEL SEGMENT

For the Fraenkel chain, the simulations of stress components as a function of time step following a step shear deformation are done in the same way as for obtaining the relaxation modulus $G_S(t)=-S_{xy}(t)/\lambda$ in Paper I. As shown in Fig. 2, the $G_S(t,\lambda)$ curves obtained for a five-bead chain at different strains from $\lambda=0.5$ to 4 indicate that the relaxation modulus of the Fraenkel-chain model is strain dependent as opposed to $G_S(t)$ in the Rouse model being independent of the strain. However, as also shown in Fig. 2, the Lodge–Meissner relation is followed even though a nonlinear effect

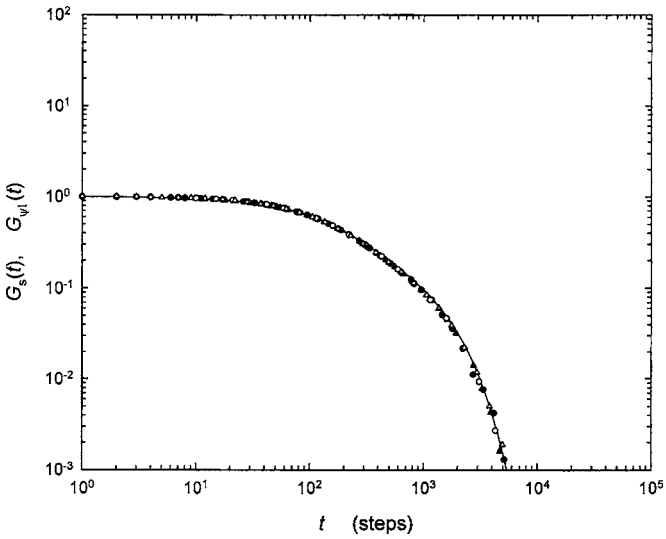

FIG. 1. Comparison of the Rouse theory (—) and the results of $G_S(t)$ (○ at $\lambda=1$; △ at $\lambda=2$) and $G_{\Psi 1}(t)$ (●at $\lambda=1$; ▲ at $\lambda=2$) obtained from simulations on the five-bead Rouse chain following the application of a step shear strain λ.

occurs in both $G_S(t,\lambda)$ and $G_{\Psi 1}(t,\lambda)$. As shown in Fig. 3, unlike in the Rouse model, the second normal-stress difference $N_2(t,\lambda)$ in the Fraenkel-chain model is not zero. Thus, the Fraenkel-chain model exhibits significant deviations in the nonlinear viscoelastic behavior from the Rouse model, even though its linear relaxation modulus in the long-time region is well described by the Rouse theory. Below, we analyze these deviations due to the particular form of the Fraenkel potential.

A large tensile force on the Fraenkel segment is created when it is significantly stretched, which leads to the stress level showing up in the fast-mode region. The strain hardening of the fast mode as shown in Fig. 2 can be understood by examining the tensile force $\mathbf{F}_F$ on a Fraenkel segment denoted by **b**:

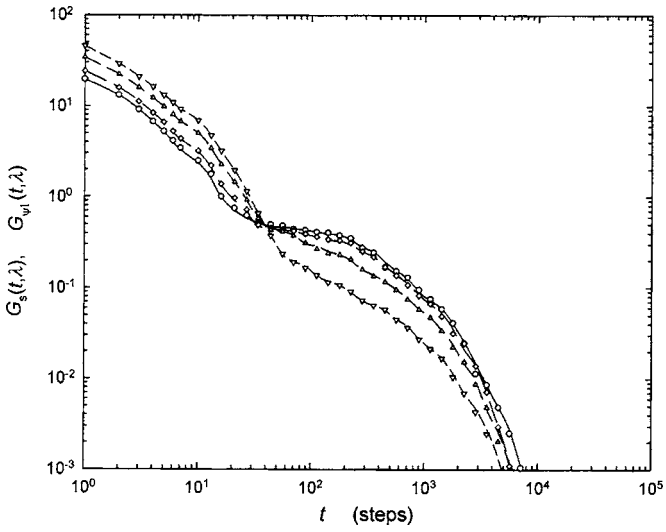

FIG. 2. Comparison of the results of $G_S(t,\lambda)$ (solid line at $\lambda=0.5$, long dash at $\lambda=1$, medium dash at $\lambda=2$, and short dash at $\lambda=4$) and $G_{\Psi 1}(t,\lambda)$ (○ at $\lambda=0.5$, ◇ at $\lambda=1$, △ at $\lambda=2$, and ▽ at $\lambda=4$) obtained from simulations on the five-bead Fraenkel chain following the application of a step shear strain λ.

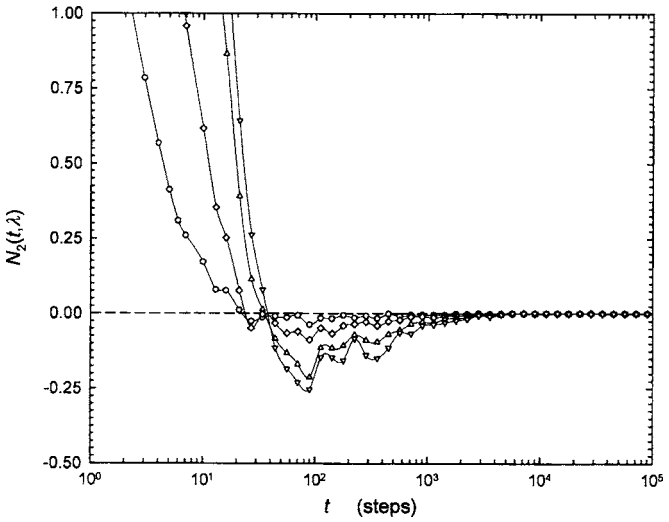

FIG. 3. Second normal stress $N_2(t,\lambda)$ obtained from simulations on the five-bead Fraenkel chain following the application of a step shear strain (○ at $\lambda=0.5$, ◇ at $\lambda=1$, △ at $\lambda=2$, and ▽ at $\lambda=4$).

$$\mathbf{F}_F = \frac{H_F}{b_0^2}\mathbf{b} - \frac{H_F}{b_0}\left[\frac{\mathbf{b}}{|\mathbf{b}|}\right] = H_F\frac{\delta(t)}{b_0^3}\mathbf{b}, \tag{4}$$

where $\delta(t)$ is defined by Eq. (16) in Paper I. As shown in Fig. 4, right after the application of a step shear to the Fraenkel chain at equilibrium, a $|\mathbf{b}(t=0_+)|$ (in this report $t=0_+$ is always used to denote the state right after the application of a step shear) value larger than b_0 (set equal to 1) in average is created; as a result, the second term of Eq. (4) becomes smaller than the first term, leading to a tensile force that would pull the two separated beads back to the equilibrium distance—a recoiling effect. In the equilibrium simulation as studied in Paper I, $\delta(t)$ is used to represent the deviation of

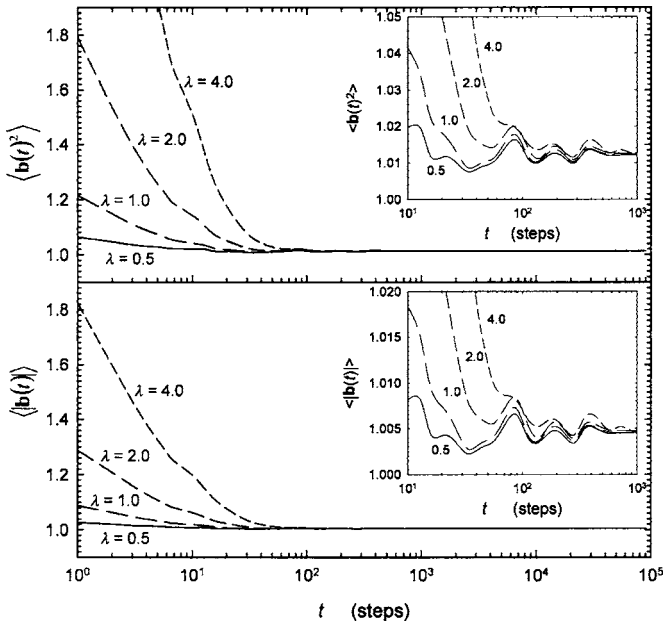

FIG. 4. $\langle \mathbf{b}(t)^2 \rangle$ (top) and $\langle |\mathbf{b}(t)| \rangle$ (bottom) as a function of time following the application of a step shear strain ($\lambda=0.5$, 1, 2, and 4) obtained from simulations on the five-bead Fraenkel chain. The insets show the oscillations in $\langle \mathbf{b}(t)^2 \rangle$ and $\langle |\mathbf{b}(t)| \rangle$ visible in the time region of 10^2-10^3 before reaching their stable equilibrium values.

the bond length $|\mathbf{b}|$ from the b_0 value in the linear region. For the present study in the nonlinear region, $\delta(t)$ is treated more as a parameter, characterizing the nonlinear enhancement of the tensile force on the segment as the segment is significantly stretched.

From close examination of the calculated values of $G_S(\lambda, t=0_+)$ as a function of strain λ (Fig. 6), nonlinear increase in the shear stress can be noticed at the shear strain λ as low as ~0.005. The average tensile force should start to increase nonlinearly greatly at $\lambda \approx 0.3$, enhancing the stress level in the fast-mode region in an obvious way. Besides this obvious expectation, this effect leads to the emergence of the second normal-stress difference. The second normal-stress difference is of significant magnitude in the fast-mode region; as the time enters the slow-mode region, it declines towards the zero line and beyond, and finally relaxes as a negative tail. This effect can be understood from the following analysis.

The use of the Langevin equation has implied that our studied system is ergodic.[5,9,10] Thus, we shall simply use the language of the ensemble averaging to discuss the results obtained from averaging the behavior of a single chain over time in the equilibrium state or over the repeating cycles following the step deformation. As obtained from the equilibrium simulation, the mean squared bond length $\langle \mathbf{b}^2 \rangle_0$ is only larger than $b_0^2=1$ by 1.3%, and the ensemble-averaged components of $\langle \mathbf{b}^2 \rangle_0$ are identical: $\langle b_x^2 \rangle_0 = \langle b_y^2 \rangle_0 = \langle b_z^2 \rangle_0 = 0.3377$. However, in the ensemble different segments have different b_x^2, b_y^2, and b_z^2 values. Among the segments with the same b_x^2, those with larger b_y^2 are expected to have a smaller b_z^2. Following the step shear deformation [Eq. 4 of Paper I], those segments with a larger b_y^2 and a smaller b_z^2 will be stretched more, leading to nonlinear enhancements in their tensile forces as characterized by the parameter $\delta(t)$, than those with a smaller b_y^2 and a larger b_z^2. Since the contribution of a segment to the normal stress in the y direction is proportional to $\delta(t)b_y(t)^2$ at time t, the average of the initial value $\delta(0_+)b_y(0_+)^2$ (right after the application of the step strain) is much more weighted by those segments with larger b_y^2; the opposite can be said about the normal stress in the z direction. As a result, the effect leads to a positive second normal-stress difference, $N_2(t)>0$, in the short-time or fast-mode region, as shown in Fig. 3. Such an effect will not occur to a Rouse segment, whose tensile force increases with bond length linearly.

As explained above, the segmental tensile force created by the step deformation will shrink the segmental length back to its equilibrium value. Those segments with a larger initial y component, having larger tensile forces, will be most affected by the recoiling effect. The average values $\langle b_x(0_+)^2 \rangle$, $\langle b_y(0_+)^2 \rangle$, and $\langle b_z(0_+)^2 \rangle$ in accordance with the affine deformation are expected to be given respectively by $\langle b_x^2(t=0_+) \rangle = \langle b_x^2 \rangle_0 + \lambda^2 \langle b_y^2 \rangle_0 = 0.3377(1+\lambda^2)$, $\langle b_y^2(t=0_+) \rangle = \langle b_y^2 \rangle_0 = 0.3377$, and $\langle b_z^2(t=0_+) \rangle = \langle b_z^2 \rangle_0 = 0.3377$. These values obtained from the simulations are in close agreement with the expected values at different strains. As the chain configuration evolves according to the Langevin equation, the recoiling effect causes all the $\langle b_x(t)^2 \rangle$, $\langle b_y(t)^2 \rangle$, and $\langle b_z(t)^2 \rangle$ values to decline,

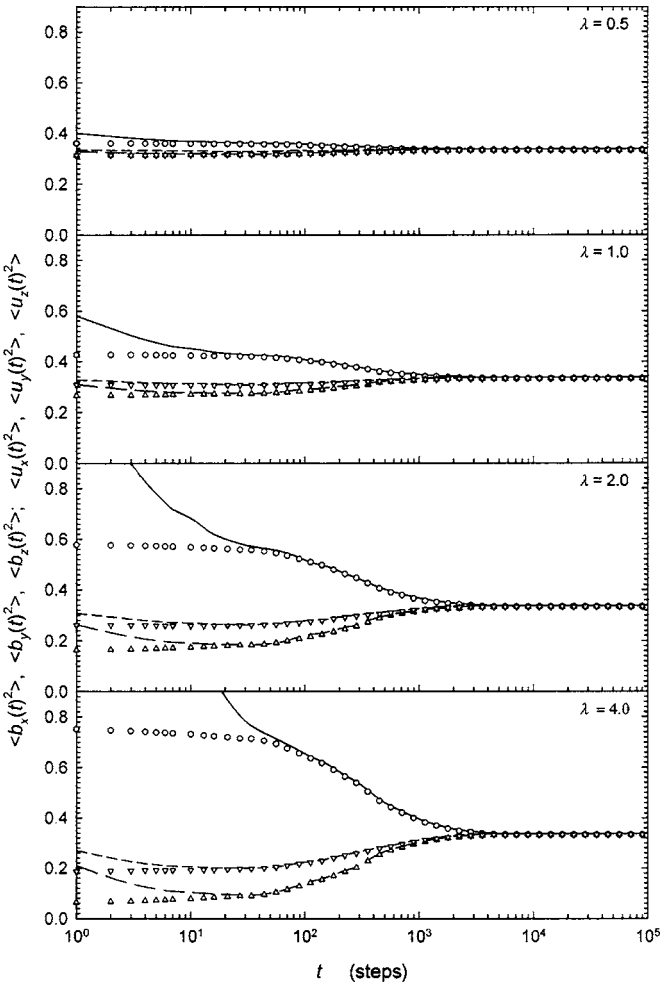

FIG. 5. $\langle b_x(t)^2\rangle$ (solid line), $\langle b_y(t)^2\rangle$ (long dash), and $\langle b_z(t)^2\rangle$ (short dash), and $\langle u_x(t)^2\rangle$ (○), $\langle u_y(t)^2\rangle$ (△), and $\langle u_z(t)^2\rangle$ (▽) as a function of time following the application of a step shear strain ($\lambda=0.5$, 1, 2, and 4) obtained from simulations on the five-bead Fraenkel chain.

as shown in Fig. 5. Due to the nonlinearly enhanced initial tensile force associated with segments with larger b_y^2, $\langle b_y(t)^2\rangle$ decreases faster than $\langle b_z(t)^2\rangle$ as $\langle \mathbf{b}(t)^2\rangle$ approaches its equilibrium value at a time which is about the end of the fast mode, as shown in Fig. 4. As $\langle \mathbf{b}(t)^2\rangle$ reaches or comes very close to its equilibrium value, $\langle b_y(t)^2\rangle$ and $\langle b_z(t)^2\rangle$ reach their respective minimum points (at around 20–40 time steps), meaning the ending of recoiling. Due to its fast declining rate from the very beginning,$\langle b_y(t)^2\rangle$ is smaller than $\langle b_z(t)^2\rangle$ at the end of the recoiling process. Thus, at about this point the second normal-stress difference $N_2(t,\lambda)$ crosses the zero line and becomes negative. In the time region corresponding to the early part of the slow mode, even though there is a significant degree of segmental-orientation anisotropy, the tensile force on the segment (as reflected by $\langle \mathbf{b}(t)^2\rangle$ or $\langle|\mathbf{b}(t)|\rangle$; see the insets of Fig. 4) is oscillating in a small magnitude around the value identical to that observed in an equilibrium state. As mentioned in Paper I, the small overshooting (only observed at $\lambda=0.5$ and 1) and damped oscillations should be the aftereffects of the recoiling of the stretched segment. As a result, as shown in Fig. 3, the second normal stress differences in the region are of small magnitude and, being most sensitive to the small changes in the tensile force on the segment, show some waviness. One can observe most clearly in the time region of 10^2-10^3 that when $\langle \mathbf{b}(t)^2\rangle$ or $\langle|\mathbf{b}(t)|\rangle$ is at the crests of its oscillation, $|N_2(t,\lambda)|$ is also at the crests of its wavy form (see Fig. 3). (Also see Fig. 9; the waviness showing up in $|N_2(t,\lambda)|$ but not in $\langle b_y(t)^2\rangle-\langle b_z(t)^2\rangle$ or $\langle u_y(t)^2\rangle-\langle u_z(t)^2\rangle$ indicates that the cause is the oscillation in the tensile force on the segment.) The above described mechanism of the chain dynamics as revealed in the results shown in Figs. 2–5 becomes more prominently visible as the applied strain λ increases.

IV. THE LODGE–MEISSNER RELATION FOR THE FRAENKEL CHAIN

The relation $G_S(t,\lambda)=G_{\Psi 1}(t,\lambda)$ first proposed by Lodge and Meissner was based on a phenomenological argument.[8] However, the Lodge–Meissner relation observed for the Fraenkel-chain model from the simulation as shown in Fig. 2 can be proved analytically. This is done by considering the configurations of all the chains in a finite volume V as changed by the applied step deformation and their subsequent evolution.

Consider a volume containing n Fraenkel chains, each with N beads. Right after the application of a step shear deformation $\mathbf{E}$ [Eq. 4 of Paper I] to a system at equilibrium, the shear stress,$-\sigma_{xy}(0_+)$, is given by (setting $kT=1$)

$$-\sigma_{xy}(0_+)=\frac{n(N-1)}{V}\langle T_x(0_+)b_y(0_+)\rangle$$

$$=\frac{H_F}{Vb_0^3}\sum_k^n\sum_s^{N-1}\delta_s^k(\lambda)(b_{s,x}^{0,k}+\lambda b_{s,y}^{0,k})(b_{s,y}^{0,k}), \tag{5}$$

where T_x denotes the x component of the tensile force $\mathbf{F}_F$ on a representative Fraenkel segment in the ensemble; $b_{s,\alpha}^{0,k}(\alpha=x,y)$ denotes specifically the α component of the sth segment on the kth chain of the system in an equilibrium state right before the application of the deformation $\mathbf{E}$. Because of the presence of $\delta_s^k(\lambda)$, which depends on the applied strain and the orientation of the segment, the summation of the terms containing the products of $b_{s,x}^{0,k}$ and $b_{s,y}^{0,k}$ over all segments is not zero. In the Rouse model, as $\delta_s^k(\lambda)$ is a constant, the sum equals zero. Because at equilibrium $\langle \mathbf{b}^2\rangle=1.013b_0^2$, we may conveniently regard each segment as having a unit length before the initial step deformation is applied (the unit length is not a required assumption to prove the Lodge–Meissner relation as given below for the Fraenkel-chain model; see Ref. 11), and the stress component as given by Eq. (5) but normalized to that for a single segment [denoted by $-S_{xy}(0_+)$] can be expressed by

$$-S_{xy}(0_+)=H_F\langle\delta(\lambda)(u_x^0u_y^0+\lambda u_y^0u_y^0)\rangle_{\mathbf{u}^0}, \tag{6}$$

where

$$\delta(\lambda)=1-\frac{1}{\sqrt{(u_x^0+\lambda u_y^0)^2+(u_y^0)^2+(u_z^0)^2}}, \tag{7}$$

with u_x^0, u_y^0 and u_z^0 denoting the x, y, and z components of a unit vector $\mathbf{u}^0$ representing the orientation of a segment in the system at equilibrium right before the step shear deformation

is applied; and $\langle f\rangle_{\mathbf{u}^0}$ denotes averaging f over all orientations of $\mathbf{u}^0$.

Similarly, the first normal-stress difference $-(\sigma_{xx}(0_+)-\sigma_{yy}(0_+))$ can be expressed by

$$-(\sigma_{xx}(0_+)-\sigma_{yy}(0_+)) = \frac{n(N-1)}{V}(\langle T_x(0_+)b_x(0_+)\rangle - \langle T_y(0_+)b_y(0_+)\rangle) = \frac{H_F}{Vb_0^3}\sum_k^n\sum_s^{N-1}[\delta_s^k(\lambda)(b_{s,x}^{0,k}+\lambda b_{s,y}^{0,k})(b_{s,x}^{0,k}+\lambda b_{s,y}^{0,k}) - \delta_s^k(\lambda)(b_{s,y}^{0,k})^2]. \quad (8)$$

In the same way as obtaining Eq. (6), the first normal-stress difference normalized to that for a single segment can be expressed by

$$N_1(0_+) = -(S_{xx}(0_+)-S_{yy}(0_+)) = H_F\langle\delta(\lambda)(u_x^0+\lambda u_y^0)(u_x^0+\lambda u_y^0)-\delta(\lambda)(u_y^0)^2\rangle_{\mathbf{u}^0}, \quad (9)$$

which, as shown in the Appendix, can be rewritten as

$$N_1(0_+) = H_F\lambda\langle\delta(\lambda)(u_x^0u_y^0+\lambda u_y^0u_y^0)\rangle_{\mathbf{u}^0} = -\lambda S_{xy}(0_+). \quad (10)$$

As there is one-to-one correspondence between the orientation representation and the segmental (molecular) representation—i.e., between Eqs. (5) and (6) and between Eqs. (8) and (9)—the contribution of $\Sigma_k^n\Sigma_s^{N-1}\delta_s^k(\lambda)[(b_{s,x}^{0,k})^2-(b_{s,y}^{0,k})^2+\lambda b_{s,x}^{0,k}b_{s,y}^{0,k}]$, corresponding to Eq. (A1), has to be zero; in other words, corresponding to Eq. (10), Eq. (8) may be rewritten as

$$-(\sigma_{xx}(0_+)-\sigma_{yy}(0_+)) = \frac{H_F}{Vb_0^3}\lambda\sum_k^n\sum_s^{N-1}\delta_s^k(\lambda)(b_{s,x}^{0,k}+\lambda b_{s,y}^{0,k})(b_{s,y}^{0,k}). \quad (11)$$

The comparison of Eqs. (5) and (11) indicates that both the shear stress and the first normal-stress difference arise from the same molecular source $\Sigma_k^n\Sigma_s^{N-1}\delta_s^k(\lambda)(b_{s,x}^{0,k}+\lambda b_{s,y}^{0,k})(b_{s,y}^{0,k})$; therefore, the same evolutions of the corresponding configurations are responsible for their relaxations. As $N_1(0_+)=-\lambda S_{xy}(0_+)$ [Eq. (10)], the Lodge–Meissner relation is followed. The above analysis can be more easily applied to the Rouse model, in which $N_1(0_+)=\lambda^2G_S(0_+)$ and $-S_{xy}(0_+)=\lambda G_S(0_+)$. As opposed to $G_S(t)$ and $G_{\Psi 1}(t)$ being independent of strain as given by Eqs. (2) and (3) for the Rouse chain model, $G_S(t,\lambda)$ and $G_{\Psi 1}(t,\lambda)$ as defined by

$$G_S(t,\lambda) = -\frac{S_{xy}(t,\lambda)}{\lambda}, \quad (12)$$

$$G_{\Psi 1}(t,\lambda) = \frac{N_1(t,\lambda)}{\lambda^2} \quad (13)$$

have the same strain dependence as shown in Fig. 2. The initial values: $G_S(t=0_+,\lambda)$ or $G_{\Psi 1}(t=0_+,\lambda)$ at different λ may be calculated numerically using Eq. (6) or (10) (i.e., performing the averaging over all orientations) for comparison with the values obtained from the simulations, as shown in Fig. 6. As also shown in the figure, the calculated curve may be further improved by the multiplication of the correction factor $\langle\mathbf{b}^2\rangle_0/b_0^2=1.013$. The close agreement between simulations and numerical calculations as shown in Fig. 6 and the agreement between the simulation results of $G_S(t,\lambda)$ and $G_{\Psi 1}(t,\lambda)$ as shown in Fig. 2 confirm the above theoretical analysis.

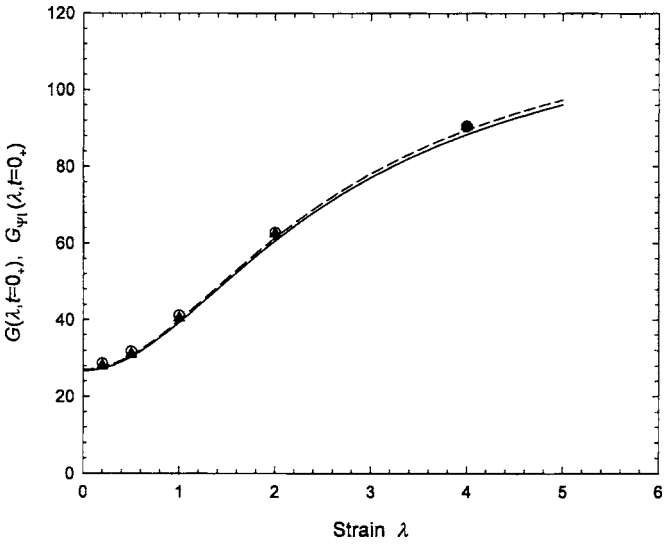

FIG. 6. Comparison of the initial values $G_S(t=0_+,\lambda)$ (○) and $G_{\Psi 1}(t=0_+,\lambda)$ (▲) obtained from simulations on the five-bead Fraenkel chain with the λ-dependent curve calculated numerically using Eq. (6) and (10) (—); the (– – –) line indicating the λ-dependent curve corrected for the ratio $\langle\mathbf{b}^2\rangle_0/b_0^2=1.013$.

Only after an averaging so complete that $\Sigma_k^n\Sigma_s^{N-1}\delta_s^k(\lambda)\times[(b_{s,x}^{0,k})^2-(b_{s,y}^{0,k})^2+\lambda b_{s,x}^{0,k}b_{s,y}^{0,k}]\to 0$, Eq. (8) becomes the same as Eq. (11). Before this is fully realized, $G_{\Psi 1}(t,\lambda)$ should show a higher noise level than $G_S(t,\lambda)$ as indeed observed in the simulation. Thus, by the Monte Carlo simulations the Lodge–Meissner relation is shown followed only within some noise.

The second normal-stress difference as a function of time obtained from the simulation of the Fraenkel chain is nonzero, as shown in Fig. 3. It can be similarly shown that the initial value of the second normal-stress difference

$$N_2(0_+) = -(S_{yy}(0_+)-S_{zz}(0_+)) = H_F\langle\delta(\lambda)((u_y^0)^2-(u_z^0)^2)\rangle_{\mathbf{u}^0} \quad (14)$$

is nonzero.

V. STRESS AND SEGMENTAL ORIENTATION

It was shown in Paper I, studying the linear viscoelastic response of the Fraenkel chain, that the slow mode reflects the fluctuation or randomization of the segmental orientation anisotropy, with the bond length being the same as in an equilibrium state; therefore, the slow mode is an entropy-driven dynamic process. Here we show that at the nonlinear strains studied (from $\lambda=0.5$ to 4), the strong correlation between the stress and the segmental orientation is well maintained in the slow-mode region. In Fig. 7 we show the comparison of the time dependences of $-S_{xy}(t)$, $\langle b_x(t)b_y(t)\rangle$, and $\langle u_x(t)u_y(t)\rangle$; in Fig. 8, the comparison of $N_1(t)$, $\langle b_x(t)^2\rangle$

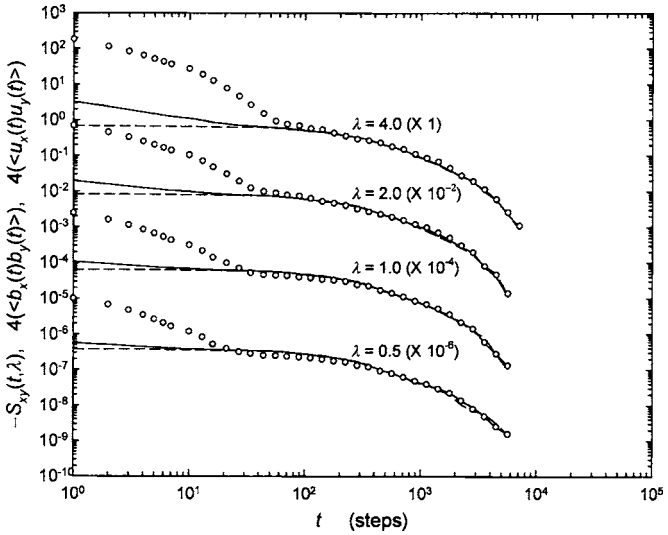

FIG. 7. Comparison of the time dependences of $-S_{xy}(t,\lambda)$ (○), $4\langle b_x(t)b_y(t)\rangle$ (—), and $4\langle u_x(t)u_y(t)\rangle$ (---) obtained from simulations on the five-bead Fraenkel chain at different λ (0.5, 1, 2, and 4). To avoid overlapping between curves, the results at different λ values have been shifted along the vertical axis by the indicated factors.

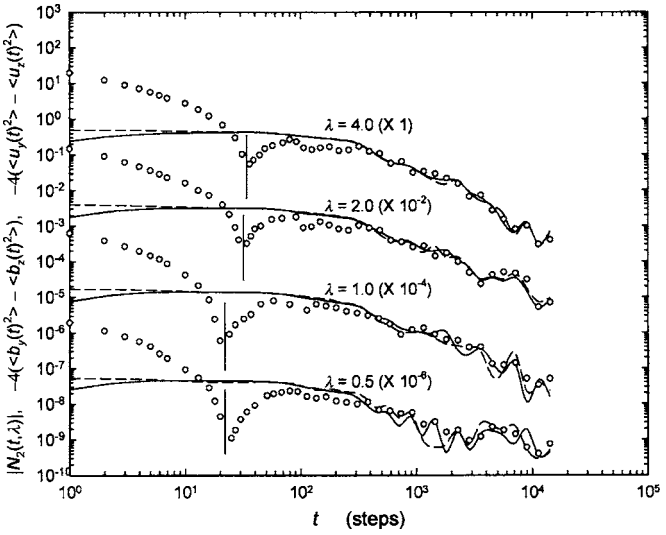

FIG. 9. Comparison of the time dependences of $|N_2(t,\lambda)|$ (○), $-4(\langle b_y(t)^2\rangle - \langle b_z(t)^2\rangle)$ (—), and $-4(\langle u_y(t)^2\rangle - \langle u_z(t)^2\rangle)$ (---) obtained from simulations on the five-bead Fraenkel chain at different λ (0.5, 1, 2, and 4); the vertical lines indicate the points where $N_2(t,\lambda)$ changes sign. To avoid overlapping between curves, the results at different λ values have been shifted along the vertical axis by the indicated factors.

$-\langle b_y(t)^2\rangle$, and $\langle u_x(t)^2\rangle - \langle u_y(t)^2\rangle$; and in Fig. 9, the comparison of $|N_2(t)|$, $\langle b_y(t)^2\rangle - \langle b_z(t)^2\rangle$, and $\langle u_y(t)^2\rangle - \langle u_z(t)^2\rangle$. The most important feature of these results is that in the slow-mode region, the stress components are proportional to the corresponding orientation components by about the same factor of 4 in all cases, which can be concisely denoted by

$$-\mathbf{S}(t,\lambda) = 4\langle \mathbf{b}(t,\lambda)\mathbf{b}(t,\lambda)\rangle \tag{15}$$

or

$$-\mathbf{S}(t,\lambda) = 4\langle \mathbf{u}(t,\lambda)\mathbf{u}(t,\lambda)\rangle, \tag{16}$$

with the difference between $\langle \mathbf{b}(t)\mathbf{b}(t)\rangle$ and $\langle \mathbf{u}(t)\mathbf{u}(t)\rangle$ being negligibly small. In the case of the Rouse theory, it is expected to have

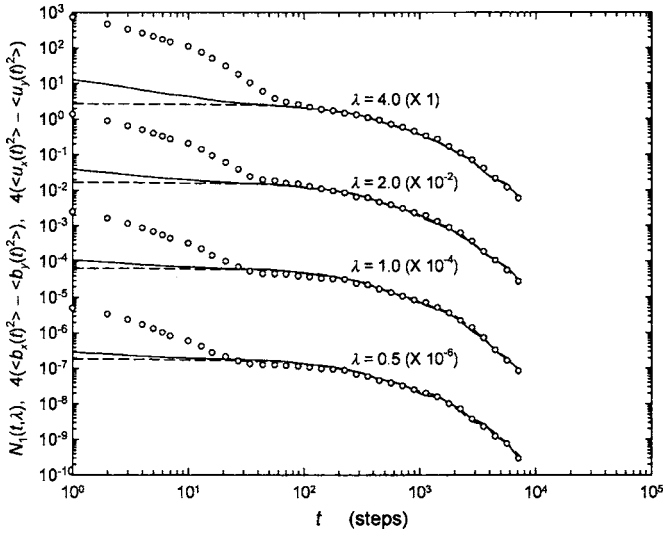

FIG. 8. Comparison of the time dependences of $N_1(t,\lambda)$ (○), $4(\langle b_x(t)^2\rangle - \langle b_y(t)^2\rangle)$ (—), and $4(\langle u_x(t)^2\rangle - \langle u_y(t)^2\rangle)$ (---) obtained from simulations on the five-bead Fraenkel chain at different λ (0.5, 1, 2, and 4). To avoid overlapping between curves, the results at different λ values have been shifted along the vertical axis by the indicated factors.

$$-\mathbf{S}(t,\lambda) = 3\langle \mathbf{b}(t,\lambda)\mathbf{b}(t,\lambda)\rangle. \tag{17}$$

Note that $S_{xz}(t) = S_{yz}(t) = 0$ in both Eqs. (15) [or (16)] and (17), and $S_{yy}(t) \neq S_{zz}(t)$ in Eq. (15) [or (16)], while $S_{yy}(t) = S_{zz}(t)$ in Eq. (17). The factor 4 in Eq. (15) being so close to the value 3 expected from the entropic force constant of the Rouse segment [Eq. (17)] strongly indicates the entropic nature of the slow mode. The revealed entropic nature of the slow mode is very significant considering that the Fraenkel segment is much stiffer than the Rouse segment and that the segment has been greatly stretched by the application of a strain in the nonlinear region. Of course, this is made possible by the fast relaxation of the segment tension, allowing the segment length to reach its equilibrium value while the segmental orientation anisotropy is still at a high level.

With the unit vector **u** representing the direction of the segment, we may denote the polarizability of a Fraenkel segment at equilibrium length in the direction parallel to **u** by $\alpha_\parallel$ and in the perpendicular direction by $\alpha_\perp$. Then the anisotropic part of the polarizability tensor of each Fraenkel segment may be expressed as[9,12,13]

$$\alpha_{\alpha\beta} = (\alpha_\parallel - \alpha_\perp)\left(u_\alpha u_\beta - \tfrac{1}{3}\delta_{\alpha\beta}\right). \tag{18}$$

With the polarizability anisotropy being given by Eq. (18), the relation as given by Eq. (16) means that the stress-optical law holds in the entropic region. The widely observed stress-optical law in the entropic region has been explained by assuming that the distribution of the distance between any two beads in a chain is Gaussian.[9,12] The Gaussian statistics applied to the chain conformation is also the source of the entropic force constant on a Rouse segment. Here, we show that both the existence of an entropic region in the stress relaxation and its associated stress-optical law can be satisfied by the Fraenkel-chain model without invoking the Gaussian statistics for both the segment and chain conformation. In fact, the Gaussian statistics for the chain should not

hold in the nonlinear region of strain as covered in this study, even in the entropic (long-time) region of $G_S(t,\lambda)$.

In the entropic region where the stress-optical law is valid, the orientation angle χ' of the stress ellipsoid is identical to the extinction angle χ of the birefringence; the stress relaxation corresponds to the reduction of the birefringence Δn with time.[14] Because the Lodge–Meissner relation holds over the whole time range of the stress relaxation, the orientation angle χ' remains the same in both the fast-mode and slow-mode regions. While $\chi=\chi'$ in the slow-mode region, it is not clear from the present simulation whether the same is true in the fast-mode region, as this would require the knowledge of how the polarizability changes with the elongation of the segment. However, it is very likely that the stress-optical coefficient will be quite different if another stress-optical rule holds in the fast-mode region. Inoue *et al.*[15,16] have analyzed the results of linear dynamic viscoelasticity and birefringence measurements on different polymers by using the sum of two stress-optical rules, one for the high-frequency region (glassy component, as denoted by Inoue *et al.*, occurring in the energetic-interactions region) and the other for the low-frequency region (rubbery component, as denoted by Inoue *et al.*, which occurs in the entropic region and is equivalent to the kind ordinarily encountered). The two stress-optical coefficients obtained by Inoue *et al.* are, in general, of very different magnitude and some with opposite signs; for instance, $C_R=-5\times10^{-9}$ vs $C_G=3\times10^{-11}$ for polystyrene melts.

VI. COMPARISON OF NONLINEAR RELAXATION MODULUS BETWEEN ENTANGLED POLYMER SYSTEM AND ENTANGLEMENT-FREE FRAENKEL-CHAIN SYSTEM

A. Overall line shapes of $G_S(t,\lambda)$

One may recall the two consecutive processes: the chain-tension relaxation[5,9,17–19] [theoretically denoted by $\mu_B^*(t,\mathbf{E})$ in Refs. 18 and 19] and the terminal mode [theoretically denoted by $\mu_C(t)$ in Refs. 18 and 19] occurring in the nonlinear relaxation modulus $G(t,\lambda)$ of an entanglement system (see Figs. 4–7 of Ref. 19 or Figs. 12.4–12.7 of Ref. 5); there are some interesting similarities in these two processes to the two relaxation modes in $G_S(t,\lambda)$ of the entanglement-free Fraenkel chain as revealed in the present study. To draw an analogy between the two systems, we regard each Fraenkel segment as corresponding to an entanglement strand and each bead as corresponding to a slip link (as in the Doi–Edwards model[20]). As what we intend to discuss is mainly an analogy, there are significant differences between the counterparts: For instance, a particularly strong chain tension on an entanglement strand will draw segments from neighboring entanglement strands, slipping through the entanglement links, while uneven tension in the Fraenkel chain is basically localized in each segment (see Ref. 21). The tensile force on the Fraenkel segment is quite large—proportional to H_F/b_0 [see Eq. (4)], which is much greater than $3kT/b_0$—while the tensile force on an entanglement strand is typically of the order $\approx 3kT/a$, with $a(>b_0)$ being the entanglement distance.[5,9,20] Thus, in applying the models to an experiment, the segment-tension relaxation of the Fraenkel chain would occur in the short-time region of $G(t,\lambda)$ with a very high modulus [for example, in the case of polystyrene, $G(t,\lambda\to0)$ in the short-time region has modulus values of $4\times10^7-10^{10}$ dynes/cm^2, which are much larger than the plateau modulus G_N, 2×10^6 dynes/cm^2,[22] occurring in a longer-time region; the plateau modulus is related to the entanglement molecular weight by $G_N=4\rho RT/5M_e$), while the chain-tension relaxation $\mu_B^*(t,\mathbf{E})$ with a modulus similar in magnitude to the plateau modulus occurs in the time region corresponding to the plateau region of the linear $G(t)$ (see Figs. 12.3 and 12.8 of Ref. 5). In spite of these differences, the similarity of showing two-step relaxation in the $G(t,\lambda)$ line shape between the two cases is obvious. Furthermore, of great interest and importance is the common effect that occurs in both the processes following the two different kinds of tension relaxation processes—namely, the terminal mode in the entangled polymer case and the slow mode in the entanglement-free Fraenkel-chain case. A discussion of the effect may shed light on the basic nature of the physics affecting a wide time/frequency range of polymer viscoelasticity. Following the process of either the segment-tension relaxation or chain-tension relaxation, it is the randomization of orientation anisotropy that is responsible for the relaxation of the remaining stress. In the entanglement-free Fraenkel-chain case, the randomization of the segmental-orientation anisotropy is caused directly by the Brownian motion of the beads in the chain, while in the entangled polymer system, the orientation associated with the entanglement strand (or primitive step) is randomized by the reptation mechanism moving the primitive chain back and forth and eventually out of the deformed (or oriented) tube (of the Doi–Edwards model), with assistance from the chain contour-length fluctuation process.[5,18,19,23,24] Either of the two different orientation-randomization processes is an entropy-driven process: In the Fraenkel-chain case, the process is well described by the Rouse model as shown in paper I (also see Fig. 10), while in the case of an entangled polymer system, the process is well described by the $\mu_C(t)$ process in the extended reptation model,[5,18,19,23,24] with the strain dependence of the modulus quantitatively described by the damping function of the Doi–Edwards theory.[5,9,18–20,25,26] As it turns out, the strain dependence of $G_S(t,\lambda)$ in the entropic region of the Fraenkel chain also closely follows the Doi–Edwards damping function for a different physical reason as analyzed in the following.

B. Damping factor in the entropic region of $G_S(t,\lambda)$

As shown in Fig. 10, the entropic region of the Fraenkel-chain $G_S(t,\lambda)$ curves at different λ values can be superposed on one another very well by a vertical shift, allowing the damping factors $h(\lambda)$ to be defined and determined from the simulation results. That is,

$$h(\lambda)=\left[\frac{G_S(t,\lambda)}{G_S(t,\lambda\to0)}\right], \tag{19}$$

with t spanning only the slow-mode region. At the same time, the damping factor is closely related to the strain de-

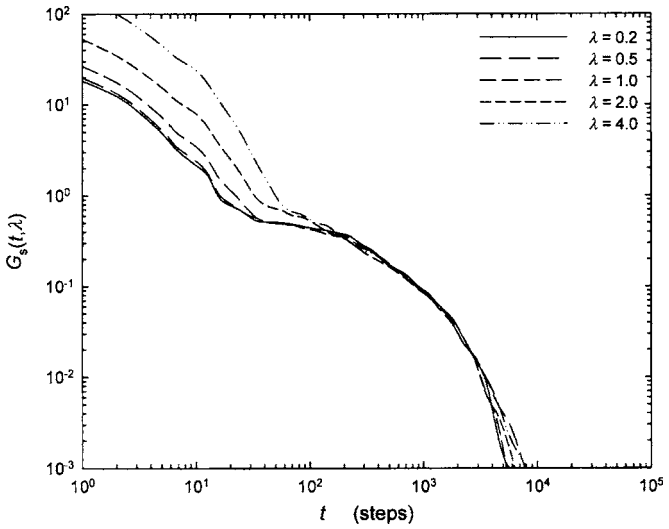

FIG. 10. Superposition of the $G_S(t,\lambda)$ curves at different strains obtained from simulations on the five-bead Fraenkel chain as shown in Fig. 2 by an upward vertical shift (multiplied by 1 at $\lambda=0.2$ and 0.5, 1.1 at $\lambda=1$, 1.5 at $\lambda=2$, and 3.5 at $\lambda=4$).

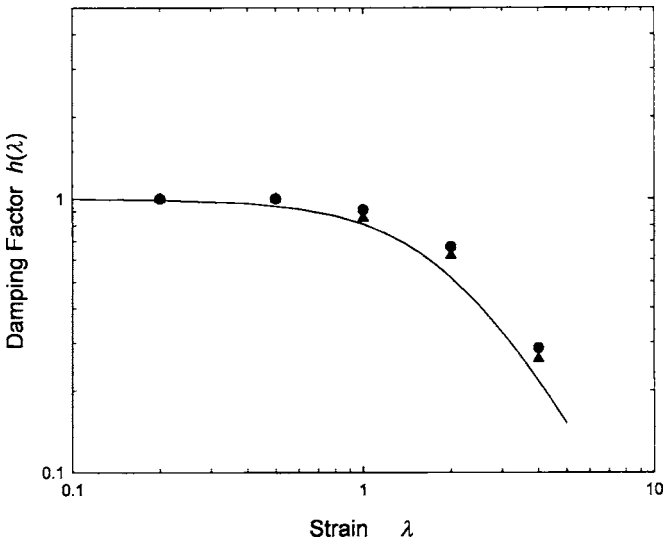

FIG. 11. Comparison of the damping factors $h(\lambda)$ (●) determined using Eq. (19) from simulations on the five-bead Fraenkel chain at different λ with the $h_0(\lambda)$ curve calculated numerically from Eqs. (20) and (21), Also shown are the values of $h_u(\lambda)$ (▲) [Eq. (22)] obtained from the simulations.

pendence of the orientation tensor $\langle \mathbf{u}(t,\lambda)\mathbf{u}(t,\lambda)\rangle$ in the entropic region as indicated by Eq. (16). As shown in Figs. 7–9, $\langle \mathbf{u}(t,\lambda)\mathbf{u}(t,\lambda)\rangle$ in the very early part of the entropic region remains basically the same as it is right after the application of the step strain; in other words, the randomization of the segmental orientation has hardly taken place as the fast mode completes its relaxation—i.e., during the recoiling of segments back to the equilibrium length. Thus the obtained damping factors $h(\lambda)$ should be closely correlated with the function $h_0(\lambda)$ calculated from the initial orientation caused by the step strain via affine deformation:

$$h_0(\lambda) = \frac{g(\lambda)}{g(\lambda \to 0)}, \tag{20}$$

with

$$g(\lambda) = \left\langle \frac{(u_x^0 + \lambda u_y^0)u_y^0}{\lambda((u_x^0 + \lambda u_y^0)^2 + (u_y^0)^2 + (u_z^0)^2)} \right\rangle_{\mathbf{u}^0}. \tag{21}$$

From Eq. (21), one obtains $g(\lambda\to 0)=0.2$. One can notice that Eqs. (20) and (21) simply define the damping function of the Doi–Edwards theory with the independent-alignment approximation, which is close to the exact one over the whole range of strain λ, both explaining very well the experimental results obtained in the terminal region of $G(t,\lambda)$ of a well-entangled nearly monodisperse polymer system.[5,9,18–20,25,26] Note that the unit vector **u** here represents the orientation of a Fraenkel segment as opposed to representing the orientation associated with an entanglement strand or primitive step in the Doi–Edwards theory. While Eq. (20) serves as an approximation to the exact expression in the Doi–Edwards theory,[5,9,18–20,25,26] using them here is based on the observation (Figs. 7–9) that the relaxation strength of the slow mode is basically directly related to the initial orientation as explained above. In Fig. 11, we compare the $h_0(\lambda)$ curve calculated numerically from Eqs. (20) and (21), and the $h(\lambda)$ values—as defined by Eq. (19)—determined from the superposition of the $G(t,\lambda)$ curves as shown in Fig. 10. As the difference between $h(\lambda=0.2)$ and $h(\lambda=0.5)$ is very small, and the numerically calculated results indicate that $h_0(\lambda=0.2)$ is only smaller than $h_0(\lambda\to 0)$ by 1%, we have substituted $h(\lambda=0.2)$ for the role of $h(\lambda\to 0)$ in determining $h(\lambda)$ at different values of λ. As shown, $h_0(\lambda)$ has basically described the trend of change in $h(\lambda)$ with increasing strain.

It is interesting and important to note that, as opposed to the similarity between their relationships to orientation as both can be characterized by the damping function given by Eqs. (20) and (21), the functional forms of relaxation modulus in the entanglement-free Fraenkel-chain case and in the entangled system are very different. The relaxation strength in the former case receives equal contributions from all normal modes [see Eq. (2)], while in the latter case is dominated by the lowest normal mode [see Eq. (13) of Ref. 19 or Eq. (9.11) of Ref. 5].

In Fig. 11, we also show the comparison of $h_0(\lambda)$ with the damping factor associated directly with the unit vector **u** in the entropic region, $h_u(\lambda)$, defined by

$$h_u(\lambda) = \frac{\langle u_x(t,\lambda)u_y(t,\lambda)\rangle/\lambda}{[\langle u_x(t,\lambda)u_y(t,\lambda)\rangle/\lambda]_{\lambda\to 0}}. \tag{22}$$

More directly representing the orientation, the $h_u(\lambda)$ values appear to have a closer agreement with $h_0(\lambda)$ than $h(\lambda)$. The small differences between $h_u(\lambda)$ and $h(\lambda)$, less than 10%, merely reflect the small deviations of the proportional constant in Eq. (16) from being exactly the same for all strains. These small differences, which may arise from the fluctuations in simulations or hidden approximations that may be involved in the interpretation, do not affect the basic physics that the slow mode as well as its entropic nature is closely correlated with the segmental-orientation anisotropy.

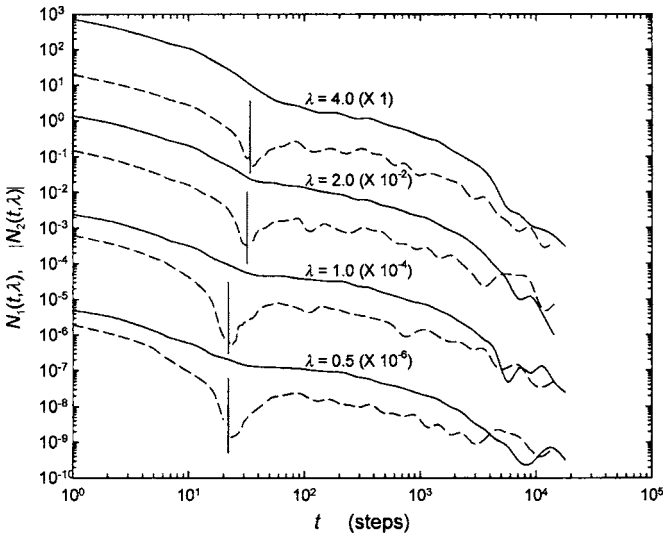

FIG. 12. Comparison of the $N_1(t,\lambda)$ (—) and $|N_2(t,\lambda)|$ (– – –) results obtained from simulations on the five-bead Fraenkel chain at different strains (λ=0.5, 1, 2, and 4); the vertical lines indicate the points where $N_2(t,\lambda)$ changes sign. To avoid overlapping between curves, the results at different λ values have been shifted along the vertical axis by the indicated factors.

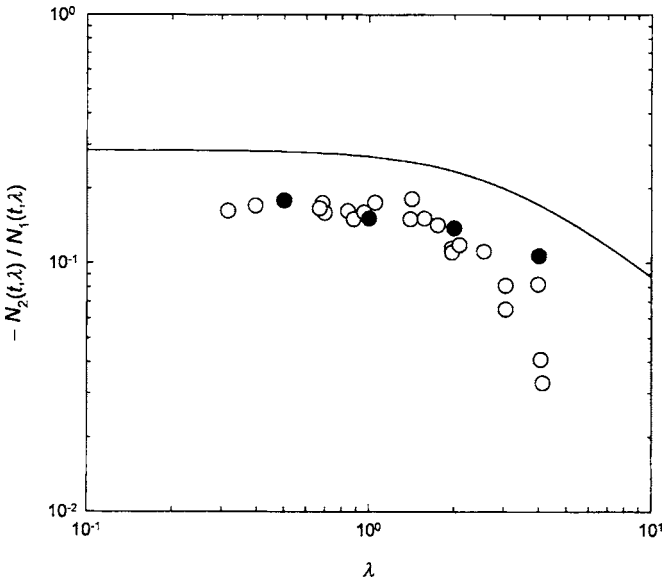

FIG. 13. Comparison of the simulation values (●) of $-N_2(t,\lambda)/N_1(t,\lambda)$ in the slow-mode region obtained from the present study and the experimental values (○) in the terminal region of the entangled system studied by Osaki *et al.* (Ref. 27), with the numerically calculated curve (—) equivalent to the Doi–Edwards expression using the independent-alignment approximation.

VII. SECOND NORMAL-STRESS DIFFERENCE VERSUS FIRST NORMAL-STRESS DIFFERENCE

Experimentally the second normal-stress difference $N_2(t,\lambda)$ is, in general, much smaller than the first normal-stress difference $N_1(t,\lambda)$, so is indicated by the comparison of the two obtained from the present simulations as shown in Fig. 12. As pointed out above, as opposed to $N_1(t,\lambda)$ being positive over the whole time range, $N_2(t,\lambda)$ is negative in the entropic region. If a polymer system can be described by the Fraenkel-chain model, one may use birefringence measurements to determine the hard-to-obtain first and second normal-stress differences in the entropic region experimentally, as the stress-optical law has been shown applicable in this region (Sec. V). Interestingly, this is also the way in which Osaki *et al.*[27] have carried out a study on the stress relaxation in an entangled system. By showing that the stress-optical law is followed in the terminal-mode region [i.e., the $\mu_C(t)$ process] of an entangled nearly monodisperse polystyrene solution ($M_w=6.7\times10^5$; 32.6% in Aroclor 1248), Osaki *et al.* have studied the first and second normal-stress differences in the region by measuring the birefringence as a function of time following a step shear deformation. The second normal-stress difference in the terminal region as determined by Osaki *et al.* in comparison with the first normal-stress difference are similar to the simulation results shown in Fig. 12 in several aspects. This may not be surprising as both the terminal mode of an entangled polymer system and the slow mode of an entanglement-free Fraenkel-chain system reflect the randomization of orientation—of the entanglement strand (or primitive step) in the former case and of the segment in the latter case; the orientations in both cases can be described well by the same shear damping function calculated from Eqs. (20) and (21). Thus, even though the relaxation functional forms are very different as pointed out above, their first and second normal-stress differences are of opposite signs in the same way and their $-N_2(t,\lambda)/N_1(t,\lambda)$ ratios have nearly the same values and λ dependence. Just as the shear damping function $h_0(\lambda)$ can be calculated from Eqs. (20) and (21), the ratio $-N_2(t,\lambda)/N_1(t,\lambda)$ can be calculated from the Doi–Edwards expression with the independent-alignment approximation for comparing with the values determined from the present simulations and the experimental values obtained by Osaki *et al.*, as shown in Fig. 13. The simulation values of $-N_2(t,\lambda)/N_1(t,\lambda)$ being about 30% below the calculated curve is most likely related to the changing sign of $N_2(t,\lambda)$ upon entering the slow-mode region. In this study we have given the picture that the fast mode is dominated by the relaxation of the segment tension, while the slow mode mainly reflects the randomization of the segmental-orientation anisotropy, without saying very much about the mutual contamination of the two dynamic processes in the two modes. It is most likely that while a very small degree of randomization of segmental orientation should have taken place before the "end" of the fast mode, some residual stretching of segment may have entered the slow-mode region. As a result, in the slow-mode region, the $N_1(t,\lambda)$ value may be enhanced somewhat by the residual stretching of the segment, while an effect in the opposite direction may occur in the absolute value of $N_2(t,\lambda)$. Such an effect can be detected from the noticeable difference between the comparisons of $N_1(t,\lambda)$ and $|N_2(t,\lambda)|$ with their corresponding tensor elements derived from the segmental orientation $\langle \mathbf{u}(t)\mathbf{u}(t)\rangle$ (multiplied by 4), as shown in Figs. 8 and 9. The values of $|N_2(t,\lambda)|$ being smaller than expected from the segmental orientation occur together with the small-amplitude oscillation observed in $|N_2(t,\lambda)|$ during the early time of the slow mode, as discussed in Sec. III.

The great similarity between the present studied system and that of Osaki *et al.* is further indicated by their observation of the Lodge–Meissner relation in the whole time region

of the terminal mode. The expected result of maintaining $(2\cot 2\chi)/\lambda=1$ in the entropic region of the present studied system—expected from the holding of the Lodge–Meissner relation over the whole time range and the holding of the stress-optical rule in the entropic region—has also been clearly observed by Osaki *et al.* in the terminal-mode region (see Fig. 4 of Ref. 27). These agreements together with the agreement with respect to the damping function strongly suggest that the close correlation of the slow mode or the terminal mode as well as its entropic nature with orientation anisotropy—as of the Fraenkel segment or the primitive step in the Doi–Edwards theory—as revealed in this study is a generally valid physical concept in polymer viscoelasticity.

VIII. SUMMARY

As shown in Paper I, the slow mode in the relaxation modulus of the Fraenkel chain in both the linear and nonlinear regions of strain is well described by the relaxation functional form of the Rouse theory with correspondingly the same number of beads. However, in reference to the constitutive equation, the Fraenkel chain behaves very differently from the Rouse chain in several important aspects. While the Lodge–Meissner relation, $G_S(t,\lambda)=G_{\Psi 1}(t,\lambda)$, holds in the Fraenkel-chain model over the whole course of stress relaxation as shown both analytically and by simulation, both $G_S(t,\lambda)$ and $G_{\Psi 1}(t,\lambda)$ are strain dependent. The physical effects responsible for the strain hardening in the fast mode and the strain softening in the slow mode are studied. That the strain dependence of $G_S(t,\lambda)$ and $G_{\Psi 1}(t,\lambda)$ in the slow-mode region of the Fraenkel chain basically follows a form identical to the damping function of Doi and Edwards with the independent-alignment approximation is explained and illustrated. Furthermore, unlike being zero in the Rouse theory, the second normal-stress difference $N_2(t,\lambda)$ of the Fraenkel chain has the same sign as the first normal-stress difference $N_1(t,\lambda)$ in the fast-mode region and changes sign as it enters the slow-mode region. The cause for the sign change has been analyzed.

As the stress tensor in the slow-mode region is directly proportional to the orientation of the segment as expressed by $\langle \mathbf{u}(t)\mathbf{u}(t)\rangle$, the applicability of the stress-optical law in this region of time is indicated. If a polymer can be modeled as a Fraenkel chain, this result also indicates that the hard-to-obtain first and second normal-stress differences in the slow-mode region can be studied by the birefringence measurements as done by Osaki *et al.*[27] in the study of an entangled system. The obtained ratio $-N_2(t,\lambda)/N_1(t,\lambda)$ and its strain dependence in the slow-mode region are indistinguishable from what have been observed in the terminal-mode region by Osaki *et al.* This as well as the agreement in the damping factor has been shown closely correlated with the great similarity in orientation anisotropy between the Fraenkel segment and the entanglement strand (or primitive step). This study suggests that this close correlation of the slow mode or the terminal mode and its entropic nature with the orientation anisotropy is a generally valid physical concept in polymer viscoelasticity.

ACKNOWLEDGMENTS

This work is supported by the National Science Council (NSC 93-2113-M-009-015 and NSC 94-2113-M-009-002), and the simulations were carried out at the National Center of High-Performance Computing.

APPENDIX: THE PROOF OF THE LODGE–MEISSNER RELATION

If we can prove

$$\langle \delta(\lambda)((u_x^0)^2-(u_y^0)^2+\lambda u_x^0 u_y^0)\rangle_{\mathbf{u}^0}=0, \tag{A1}$$

then Eq. (9) becomes Eq. (10). Considering the symmetry, we have $\langle((u_x^0)^2-(u_y^0)^2+\lambda u_x^0 u_y^0)\rangle_{\mathbf{u}^0}=0$, thus, Eq. (A1) is true if

$$A(\lambda)=\left\langle \frac{(u_x^0)^2-(u_y^0)^2+\lambda u_x^0 u_y^0}{\sqrt{(u_x^0+\lambda u_y^0)^2+(u_y^0)^2+(u_z^0)^2}}\right\rangle_{\mathbf{u}^0} \tag{A2}$$

is zero for all values of λ. Both the numerator and denominator of Eq. (A2) contain even and odd terms with respect to the transformation $u_x^0\to -u_x^0$ or $u_y^0\to -u_y^0$. The averaging over all orientations of $\mathbf{u}^0$ is invariant to a rotation of the coordinate system. The way to show $A(\lambda)=0$ is to do an orthogonal transformation to Eq. (A2), making its denominator contain only even terms. This can be done by finding the principal axes for the quadratic form inside the square root of the denominator, which is simply $\mathbf{u}^0\cdot\mathbf{C}\cdot\mathbf{u}^0$, with $\mathbf{C}$ being the Cauchy tensor. With $\mathbf{C}$ represented by a matrix C:

$$C=\begin{pmatrix}1 & \lambda & 0\\ \lambda & 1+\lambda^2 & 0\\ 0 & 0 & 1\end{pmatrix} \tag{A3}$$

and the unit vector $\mathbf{u}^0$ represented by a column U:

$$U=\begin{pmatrix}u_x^0\\ u_y^0\\ u_z^0\end{pmatrix}, \tag{A4}$$

we may write

$$\mathbf{u}^0\cdot\mathbf{C}\cdot\mathbf{u}^0=U^T C U. \tag{A5}$$

Expressing the unit vector $\mathbf{u}^0$ with respect to the principal axes as

$$U'=\begin{pmatrix}u_x'\\ u_y'\\ u_z'\end{pmatrix}, \tag{A6}$$

the orthogonal transformation is given by

$$U=SU' \tag{A7}$$

with

$$S = \begin{pmatrix} \sqrt{2}/\sqrt{\mu+\lambda\sqrt{\mu}} & (-\lambda-\sqrt{\mu})/\sqrt{2}\sqrt{\mu+\lambda\sqrt{\mu}} & 0 \\ (\lambda+\sqrt{\mu})/\sqrt{2}\sqrt{\mu+\lambda\sqrt{\mu}} & \sqrt{2}/\sqrt{\mu+\lambda\sqrt{\mu}} & 0 \\ 0 & 0 & 1 \end{pmatrix}, \tag{A8}$$

where $\mu=\lambda^2+4$. In terms of u'_x, u'_y, and u'_z, Eq. (A2) is expressed by

$$A(\lambda) = \left\langle \frac{-\sqrt{\mu}u'_x u'_y}{\sqrt{q_1(u'_x)^2 + q_2(u'_y)^2 + q_3(u'_z)^2}} \right\rangle_{\mathbf{u}'}, \tag{A9}$$

where q_1, q_2, and q_3 are the three eigenvalues of C:

$$q_1 = \frac{\mu - 2 + \lambda\sqrt{\mu}}{2}, \tag{A10}$$

$$q_2 = \frac{\mu - 2 - \lambda\sqrt{\mu}}{2}, \tag{A11}$$

$$q_3 = 1. \tag{A12}$$

While the denominator of Eq. (A9) contains only even terms, the numerator is an odd term. Thus, $A(\lambda)=0$ for all λ; this leads to the result that the Lodge–Meissner relation $G_S(t,\lambda)=G_{\Psi_1}(t,\lambda)$ holds.

[1] Y.-H. Lin and A. K. Das, J. Chem. Phys. **126**, 074902 (2007), preceding paper.
[2] G. K. Fraenkel, J. Chem. Phys. **20**, 642 (1952).
[3] P. E. Rouse, Jr., J. Chem. Phys. **21**, 1272 (1953).
[4] R. B. Bird, C. F. Curtiss, R. C. Armstrong, and O. Hassager, *Dynamics of Polymeric Liquids*, 2nd ed. (Wiley, New York, 1987), Vol. 2.
[5] Y.-H. Lin, *Polymer Viscoelasticity: Basics, Molecular Theories, and Experiments* (World Scientific, Singapore, 2003).
[6] Y.-H. Lin, Macromolecules **19**, 168 (1986).
[7] Y.-H. Lin and J.-H. Juang, Macromolecules **32**, 181 (1999).
[8] A. S. Lodge and J. Meissner, Rheol. Acta **11**, 351 (1972).
[9] M. Doi and S. F. Edwards, *The Theory of Polymer Dynamics* (Oxford Univ. Press, New York, 1986).
[10] D. A. McQuarrie, *Statistical Mechanics* (Harper & Row, New York, 1976).
[11] In the ensemble, segments with a certain bond length are oriented in all directions with equal probability; this is true with any bond length that can occur in an equilibrium state. Each "group" of segments with the same bond length can be normalized in the same way and averaged over all orientations as described in the text.
[12] W. Kuhn, Kolloid-Z. **68**, 2 (1934); W. Kuhn and F. Grun, *ibid.* **101**, 248 (1942); W. Kuhn, J. Polym. Sci. **1**, 360 (1946).
[13] B. J. Berne and R. Pecora, *Dynamic Light Scattering* (Wiley, New York, 1976).
[14] H. Janeschitz-Kriegl, Adv. Polym. Sci. **6**, 170 (1969).
[15] T. Inoue, H. Okamoto, and K. Osaki, Macromolecules **24**, 5670 (1991).
[16] T. Inoue, H. Hayashihara, H. Okamoto, and K. Osaki, J. Polym. Sci., Part B: Polym. Phys. **30**, 409 (1992).
[17] M. Doi, J. Polym. Sci., Polym. Phys. Ed. **18**, 1005 (1980).
[18] Y.-H. Lin, J. Rheol. **29**, 605 (1985).
[19] Y.-H. Lin, J. Non-Newtonian Fluid Mech. **23**, 163 (1987).
[20] M. Doi and S. F. Edwards, J. Chem. Soc., Faraday Trans. 2 **74**, 1789 (1978); J. Chem. Soc., Faraday Trans. 2 **74**, 1802 (1978).
[21] Dynamic coupling between tensile forces on different segments of the same chain can occur, as indicated by the extension of the fast mode to the longer-time region with the increase of beads per chain when the applied strain is large.
[22] See *Polymer viscoelasticity: Basics, Molecular Theories, and Experiments* (Ref. 5), Chap. 13.
[23] Y.-H. Lin, Macromolecules **17**, 2846 (1984).
[24] Y.-H. Lin, Macromolecules **19**, 159 (1986); **20**, 885 (1987).
[25] K. Osaki and M. Kurata, Macromolecules **13**, 671 (1980).
[26] K. Osaki, K. Nishizawa, and M. Kurata, Macromolecules **15**, 1068 (1982).
[27] K. Osaki, S. Kimura, and M. Kurata, J. Polym. Sci., Polym. Phys. Ed. **19**, 517 (1981).